

Optimized adsorption removal and capacity prediction of anionic pollutants using a hybrid strategy of machine learning algorithms

Hamza Ul Haq¹, Muhammad Yasir^{2,*}, Muhammad Nouman Aslam Khan¹, Jawad Gul¹, Mukarram Zubair³, Hassan Ali², Vladimir Sedlarik², Nasir. M. Ahmad^{1,*}

¹Multiscale & Intelligence for Materials Innovation and Chemical Engineering, School of Chemical and Materials Engineering, National University of Sciences and Technology, Islamabad 44000, Pakistan

²Centre of Polymer Systems, Tomas Bata University in Zlin, Tr. T. Bati 5678, 76001 Zlin, Czech Republic

³Environmental Engineering Department, College of Engineering A13, Imam Abdulrahman Bin Faisal University, Main Campus, P.O. Box 1982, Dammam 34212, Saudi Arabia.

*Corresponding authors. M.Y (yasir@utb.cz) and N.M.A (nasir.ahmad@scme.nust.edu.pk)

Abstract

Accurate prediction of adsorption performance is crucial for optimizing wastewater treatment systems, however, the complex interactions among operational variables and adsorbent properties often limit conventional modelling approaches. In this study, a machine learning framework was developed to predict the adsorption removal efficiency and kinetic capacity of anionic pollutants in aqueous systems. A comprehensive experimental dataset was generated using four representative pollutants, i.e., bovine serum albumin, methyl orange, sulfate, and nitrate and four adsorbent materials, including powdered activated carbon (PAC), thermally modified PAC, chemically modified PAC, and ion-exchange chitosan beads. Key operational parameters, including pH, contact time, adsorbent dosage, BET surface area, solution volume, and pollutant concentration, were used as input features. Four ML algorithms, i.e., Decision Tree (DT), Gaussian Process Regression (GPR), Support Vector Machine (SVM), and Ensemble Learning Tree (ELT), were developed and further optimized using Bayesian optimization to improve predictive performance. Among the evaluated models, the optimized ELT model demonstrated the highest predictive accuracy with a coefficient of determination (R^2) of 0.78, indicating its strong capability in capturing nonlinear adsorption behavior. Model interpretation through partial dependence plots revealed significant influences of pH, adsorbent dosage, BET surface area, and initial pollutant concentration on adsorption performance, while Sobol sensitivity analysis confirmed the dominant role of initial concentration. Experimental validation using jojoba-derived biochar for the removal of methyl orange and Eriochrome Black T dyes showed strong agreement with model predictions. The developed ML models provide a reliable tool for predicting adsorption performance and designing efficient adsorbent-based wastewater treatment systems.

Keywords: machine learning; adsorption; anionic pollutant; wastewater treatment; adsorbent materials.

1. Introduction

Anthropogenic activities over the last century have resulted in the release of various pollutants into the environment, greatly affecting global biodiversity and humans' health alike. These pollutants, originating primarily from industrial processes, energy production, and transportation, pose grave risks to the planet's ecosystems. Water pollution, which arises mainly from the discharge of untreated industrial effluents, agricultural runoff containing pesticides and fertilizers, and domestic sewage, degrades aquatic habitats and threatens biodiversity [1]. Industries often release toxic chemicals, heavy metals, and dyes into nearby water bodies without

41 adequate treatment, while agricultural activities contribute pollutants such as fertilizers, pesticides, and animal
42 waste, which can lead to eutrophication [2,3]. This process causes excessive algal growth, depletes oxygen levels,
43 and results in the death of aquatic organisms. This uncontrolled level of environmental pollution threatens
44 environmental sustainability; therefore, tackling global environmental pollution has become one of the primary
45 goals to improve the quality of life for the entire global biodiversity of the planet [4]. Therefore, stringent
46 regulations have been implemented to prevent the unregulated release of environmental toxicants. For example,
47 the UN's Sustainable Development Goals No. 6 and 14 directly address this issue by providing guidance on how
48 to tackle it [5]. To date, various technologies have been explored to address water pollution, including
49 sedimentation [6], reverse osmosis, ozonation, ion-exchange resins, adsorption, biological treatment, and
50 advanced oxidation processes (AOPs) [7,8]. Each method provides different rates of pollutant removal efficiency
51 and flexibility. Among these techniques, adsorption is widely regarded as one of the most effective and versatile
52 technologies for removing pollutants from water, offering several advantages over other treatment methods.
53 Unlike chemical or biological treatments that may require complex reactions or specific environmental conditions,
54 adsorption is simple, efficient, and easy to operate, as it requires mainly a suitable adsorbent with high affinity to
55 adsorb pollutants to the surface, such as activated carbon [9], biochar [10], zeolites [11], or nanomaterials, without
56 altering the chemical structure of the pollutants [12]. Moreover, adsorption systems generally produce minimal
57 secondary waste, unlike other methods, which mostly generate secondary pollutants after pollutant degradation or
58 decomposition, such as from ozonation or AOPs [13]. To date, research in this field is primarily focused on
59 developing highly porous, high-surface-area materials with tailored surface chemistry to improve adsorption,
60 adsorption capacity, selectivity, kinetics, and regeneration. These materials include carbon-based materials, such
61 as carbon quantum dots and metal-organic frameworks, as well as bio-based materials [14,15]. In addition to
62 structurally engineered adsorptive materials for pollutant removal based on the preceding strategies, various
63 operational parameters also affect the rate and extent of adsorptive removal. These factors include contact time,
64 pollutant concentration, pH, solution volume, surface area, adsorbent dosage, and others [16,17]. These factors,
65 along with others, greatly influence and control the adsorptive performance of the adsorbent material. However,
66 it is challenging to analyze the influence of each factor on determining the adsorptive rate of pollutant removal,
67 as it proceeds through multivariable interactions. In this regard, an investigation into the influence of each
68 operational parameter on the adsorptive removal of pollutants can provide valuable insights into achieving highly
69 cost-effective, efficient pollutant removal with adsorbent materials.

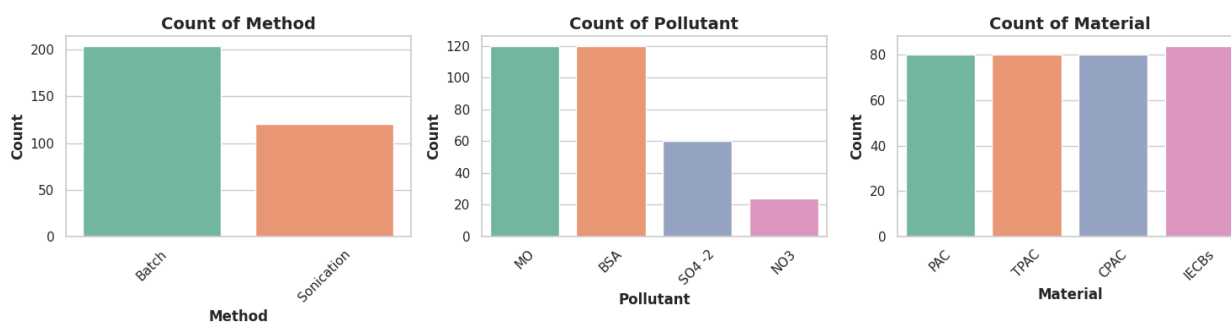
70 Fortunately, owing to recent advances in computer modelling and the implementation of machine
71 learning (ML), the complex interplay between various operational parameters can be elucidated using ML. In ML,
72 various algorithms are applied to a collected dataset to analyze patterns and draw predictions [18]. To obtain
73 highly accurate ML models that can predict required output values, it is necessary to acquire a large dataset, select
74 suitable ML models, train them, and validate them by testing them on randomly selected parameter values. So far,
75 ML has been successfully implemented in various fields, including chemistry, for materials discovery [19],
76 prediction of chemical reactions [20], optimization of reactions [21], photocatalytic dye removal optimization
77 [22], and adsorptive removal of pollutants [23]. However, the accuracy and feasibility of each ML is different
78 from application to application, with each model having its own degree of applicability, versatility, and suitability.
79 Some common ML models investigated for various use cases include decision trees (DT) [24], random forests
80 (RF) [25], support vector machines (SVM) [26], and linear regression (LR) [27]. As in the case of other chemical

81 science-based applications, the literature survey suggests that ML has been implemented to investigate various
82 aspects of the adsorptive removal of pollutants. For instance, the Venegas group reported on utilizing an ML
83 approach to predict adsorptive removal of ciprofloxacin, a highly bioactive drug detected in high concentrations
84 in wastewaters, using sugarcane bagasse biomass. Based on their experimental data, the developed ML models
85 achieved great prediction capability at both laboratory and pilot scale experiments. The authors reported optimized
86 adsorptive capacities of 2.19 mg/g and 2.53 mg/g, for laboratory and pilot scale experiments, respectively, by
87 which optimized operational parameters of both different experiments were obtained [28]. Similarly, other groups
88 have reported applying ML models to predict adsorptive removal of pollutants such as Lindane [29], organic
89 pollutants [30], and selenium [31]. However, the preceding studies, while novel themselves, have been conducted
90 on a limited scale and with a limited variety of pollutants. Therefore, considering the current state of the art in this
91 field, we report on the implementation of ML models on a large dataset to remove various anionic pollutants using
92 adsorptive materials. Four commonly encountered anionic pollutants in wastewater, i.e., bovine serum albumin
93 (BVA), methyl orange (MO), SO_4^{2-} , and NO_3^{1-} were selected, while four different adsorptive materials, i.e.,
94 powdered activated carbon (PAC), thermally modified PAC (TPAC), chemically modified PAC (CPAC), and ion
95 exchange chitosan beads (IECBs), were chosen to obtain a reliable dataset. To leverage ML models, various
96 operational influencing parameters were selected, and four ML models (DT, GPR, SVM, and ELT) were applied
97 to establish intricate relationships between the adsorptive pollutants' removal degree and these parameters. The
98 developed and trained ML models were further optimized using the Bayesian optimization technique, enabling
99 more accurate prediction of the adsorptive capacity of selected adsorptive materials by considering the influence
100 of operational parameters. The developed ML models were further experimentally validated to assess their
101 reliability by conducting adsorptive removal of pollutants using randomly selected input features, yielding high
102 predictive accuracy.

103 **2. Methodology**

104 **2.1. Data collection and pre-processing**

105 For training and testing ML models, adsorptive removal data for various adsorbents were obtained from our
106 group's laboratory experiments. Experiments were conducted by varying selected parameters to obtain a diverse
107 range of datapoints suitable for enhancing the model's training and predictive capabilities. A tabulated list of all
108 data points, together with their associated parameters, is provided in Table S1. The adsorptive experiments were
109 conducted in sonication and non-sonication (batch) modes, which can also influence the adsorptive removal
110 capacity. To keep the study's data points consistent, only commonly encountered anionic pollutants were used in
111 all experiments (Figure 1).



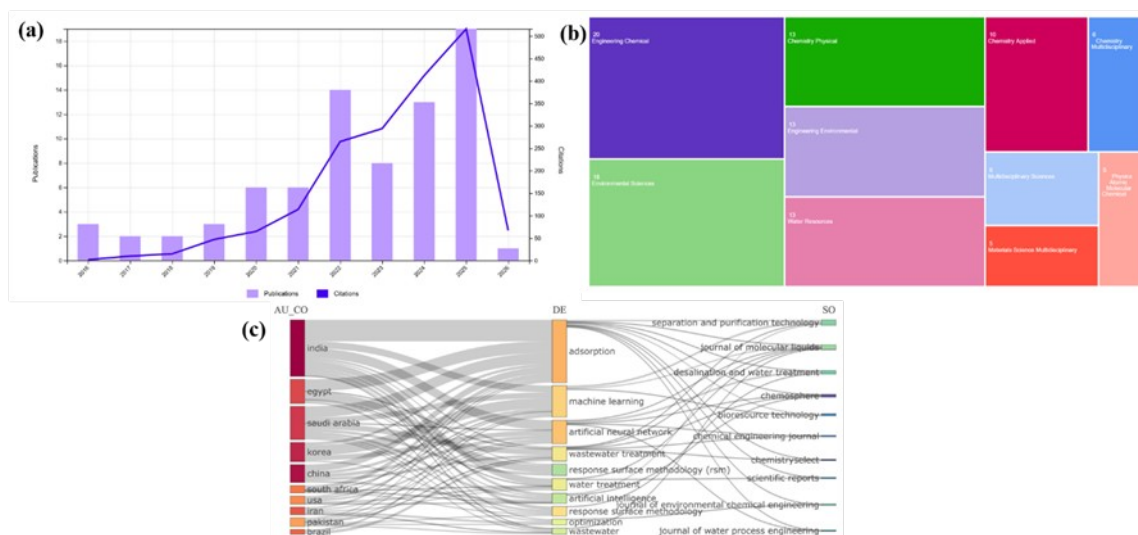
112

113 **Figure 1.** Number of counts of adsorptive removal method, pollutant, and material type utilized for training ML
 114 models.

115 **2.2. Bibliometric analysis**

116 The bibliometric analysis reveals a steadily expanding research landscape at the intersection of ML, adsorption
 117 processes, and anionic pollutants removal from wastewater systems between 2016 and 2026. As illustrated in
 118 Figure 2a, publication output remained modest during the early years (2016-2018) but began to increase
 119 significantly after 2020, with a pronounced rise in both publications and citations between 2022 and 2025. The
 120 surge in citations in later years indicates growing scholarly recognition and the consolidation of foundational
 121 studies in this domain. Although the reported annual growth rate appears statistically neutral, the visual trend
 122 clearly shows accelerated research activity in recent years, suggesting that ML-assisted adsorption research is
 123 transitioning from exploratory investigations to a more mature and structured field. The distribution of subject
 124 areas (Figure 2b) further highlights the field's interdisciplinary nature. Engineering, Chemical, and Environmental
 125 Sciences constitute the dominant categories, reflecting the strong process-engineering orientation of adsorption-
 126 based wastewater treatment studies. Concurrently, substantial contributions from Chemistry-related disciplines
 127 underscore the importance of material design, adsorbent characterization, and physicochemical interaction
 128 mechanisms. The presence of Water Resources and Engineering Environmental categories confirms that research
 129 efforts are closely aligned with sustainable water management and environmental remediation objectives.

130 The thematic and collaboration network depicted in Figure 2c provides additional insight into the intellectual
 131 structure of the field. “Adsorption,” “machine learning,” and “artificial neural network” emerge as central
 132 conceptual nodes, indicating that predictive modelling and optimization techniques are increasingly integrated
 133 into adsorption performance evaluation. Countries such as India, Egypt, Saudi Arabia, and China appear
 134 prominently in the collaboration network, suggesting that emerging economies are actively contributing to
 135 advancements in ML-driven wastewater treatment research. Furthermore, the concentration of publications in
 136 specialized journals related to separation technology, environmental engineering, and chemical processing reflects
 137 the applied and solution-oriented nature of this research area. Collectively, these findings indicate a rapidly
 138 evolving, multidisciplinary field characterized by increasing research impact, collaborative engagement, and
 139 methodological integration of artificial intelligence within environmental engineering frameworks.



140

141 **Figure 2.** Bibliometric overview of machine learning-assisted adsorption research for anion removal in wastewater treatment
 142 (2016-2026). (a) Annual publication and citation trends, (b) Subject area distribution based on Web of Science categories,
 143 and (c) Three-field plot illustrating relationships among contributing countries (AU-CO), author keywords (DE), and sources
 144 (SO).

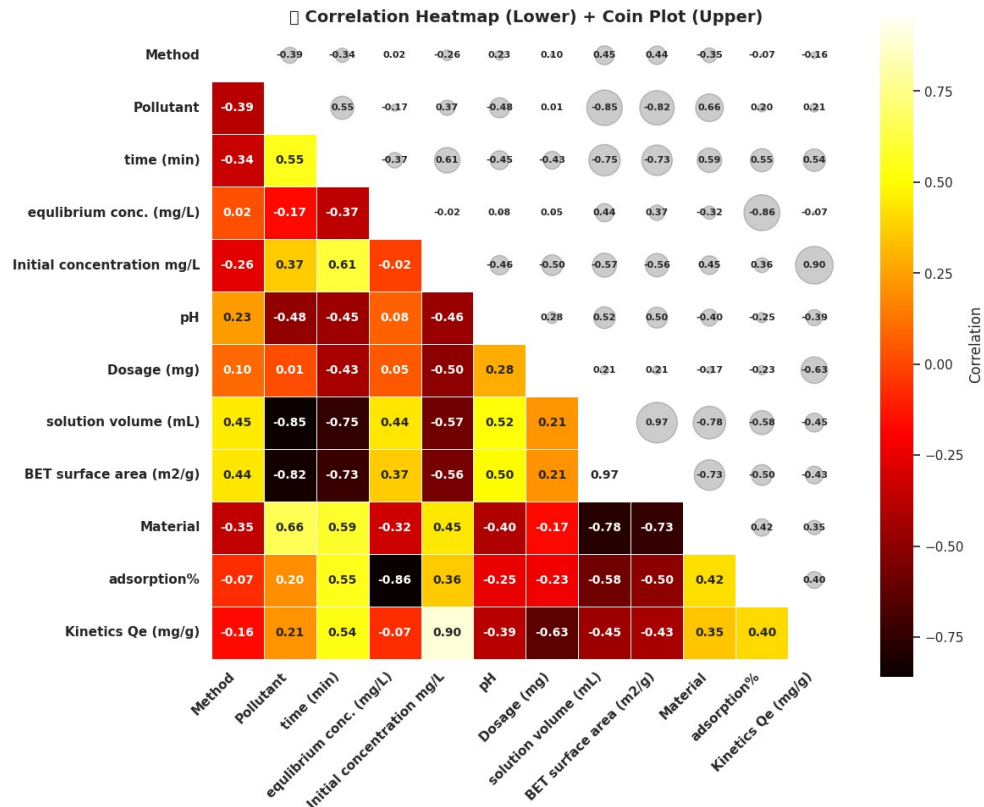
145 The keyword co-occurrence analysis provides insight into the intellectual structure and thematic evolution of ML-
 146 assisted adsorption research for anionic pollutants removal in wastewater systems. As illustrated in Figure S1a,
 147 adsorption emerges as the most dominant and central keyword, confirming its foundational role within this
 148 research domain. Closely associated terms such as removal, aqueous solution, adsorbent, and activated carbon
 149 indicate that experimental adsorption studies remain the primary research backbone. The dense interconnections
 150 among these terms highlight the continued emphasis on pollutant removal from aqueous media using engineered
 151 adsorbent materials. Importantly, ML-related terms, including machine learning, artificial neural network (ANN),
 152 and optimization are strongly integrated within the network rather than appearing as isolated clusters (Figure S1a).
 153 This suggests that predictive modelling approaches are increasingly embedded within adsorption performance
 154 evaluation frameworks. The presence of modelling-associated keywords such as response surface methodology
 155 (RSM), kinetics, and isotherm further indicates the convergence of statistical, mechanistic, and AI-based methods.
 156 Additionally, the appearance of material-oriented terms such as nanoparticles, graphene oxide, biochar, and
 157 composites reveals ongoing innovation in adsorbent design, demonstrating that computational intelligence is
 158 being applied alongside material-engineering advancements. The thematic map shown in Figure S1b further
 159 categorizes research themes according to their centrality and development density. Core topics such as adsorption,
 160 aqueous solutions, and removal are positioned within the motor theme quadrant, indicating that they are well
 161 developed and highly central to the field. These themes represent the driving intellectual forces of the research
 162 area. In contrast, foundational yet still evolving topics such as wastewater treatment, performance, and adsorption
 163 mechanisms fall within the basic theme quadrant, suggesting their essential yet developing role in sustaining
 164 research growth. Methodological themes, including response surface methodology and artificial neural networks,
 165 appear in niche or transitional areas, suggesting that although these approaches are technically well developed,
 166 their broader conceptual integration continues to expand. The placement of certain AI-related terms in emerging
 167 or transitional zones suggests a dynamic shift toward more advanced or hybrid modelling frameworks.

168 The quantitative keyword distribution presented in Figure S1c corroborates these observations. The treemap
169 clearly demonstrates that adsorption accounts for the highest frequency of occurrences, followed by aqueous
170 solution, removal, and activated carbon. The notable presence of ML, ANN, and optimization confirms the
171 increasing prominence of computational modelling within adsorption research. Moreover, frequent references to
172 model pollutants such as methylene blue, Congo red, and anionic dyes indicate that dye-removal studies remain a
173 common benchmark for evaluating adsorbent performance. This pattern suggests that while artificial intelligence
174 techniques are gaining importance, the field remains application-oriented and strongly driven by experimental
175 performance assessment.

176 **2.3. Data representation**

177 The distributions of the input and output variables used to train the machine learning models are illustrated in
178 Figure S2 using violin plots. These plots combine kernel density estimation with boxplots, providing insight into
179 the data's spread, central tendency, and density. The adsorption efficiency exhibits a broad distribution with higher
180 data density at moderate to high removal efficiencies, indicating that most reported systems achieve effective
181 adsorption under optimized conditions. BET surface area shows a broad, partially bimodal distribution, indicating
182 the use of both low- and high-porosity adsorbents across the collected studies. Experimental parameters such as
183 adsorbent dosage, solution volume, and contact time are clustered within commonly adopted ranges, while
184 sufficient variability is retained to ensure robust model learning. The initial pollutant concentration displays a
185 pronounced right-skewed distribution, spanning dilute to highly concentrated systems, whereas equilibrium
186 concentration is predominantly skewed toward lower values, consistent with efficient contaminant removal. The
187 pH distribution is multimodal, with most experiments conducted under acidic to near-neutral conditions,
188 highlighting the strong role of pH in adsorption processes. Overall, the broad yet physically meaningful
189 distributions of these variables obtained in our lab confirm the dataset's diversity and representativeness, which
190 are essential for developing reliable and generalizable machine learning models.

191 Figure 3 presents the combined correlation heatmap (lower triangle) and coin plot (upper triangle) illustrating the
192 pairwise relationships among the selected variables used utilized for training the ML models. From the figure, the
193 adsorption efficiency shows moderate positive correlations with contact time and initial pollutant concentration,
194 indicating enhanced removal performance at longer interaction times and higher driving force for mass transfer,
195 while it is negatively correlated with equilibrium concentration, consistent with effective adsorption leading to
196 lower residual concentrations. Kinetic adsorption capacity (Q_e) exhibits a strong positive correlation with the
197 initial concentration and a negative correlation with equilibrium concentration, implying typical adsorption
198 behavior governed by concentration gradients. Contact time is positively correlated with initial concentration but
199 negatively correlated with equilibrium concentration, suggesting improved pollutant uptake as exposure time
200 increases. BET surface area and solution volume display strong intercorrelation, reflecting their combined
201 influence on available adsorption sites and mass transfer conditions, while both variables show moderate
202 correlations with adsorption efficiency and kinetic capacity. Adsorbent dosage is moderately negatively correlated
203 with equilibrium concentration and positively correlated with solution volume, indicating that higher adsorbent
204 loading promotes greater pollutant removal. Overall, the correlation analysis reveals physically meaningful
205 interdependencies among operational and structural parameters, supporting their relevance as input features for
206 ML models development.



207

208 **Figure 3.** Pearson correlation and coin plot between adsorption removal and experimental conditions.

209 **2.4. Machine learning models**

210 In this study, multiple machine learning algorithms were employed to develop a hybrid predictive framework for
 211 modelling the adsorption efficiency and capacity of anionic dyes and proteins on functionalized biochar surfaces.
 212 The integration of diverse models, such as Decision Tree (DT), Ensemble Learning Tree (ELT), Gaussian Process
 213 Regression (GPR), and Support Vector Machine (SVM), enables a comprehensive learning of both linear and
 214 nonlinear adsorption behavior [32,33]. Each algorithm contributed unique computational strengths, collectively
 215 improving prediction reliability and interpretability of adsorption phenomena. Each algorithm contributed unique
 216 computational strengths, collectively improving prediction reliability and interpretability of adsorption
 217 phenomena.

218 **2.3.1 Decision Tree (DT)**

219 The decision tree algorithm was employed for its ability to provide clear interpretability and variable importance
 220 analysis. DT works by recursively partitioning the data based on decision rules that minimize prediction error,
 221 allowing straightforward identification of critical factors influencing adsorption removal and capacity. In
 222 adsorption-related research, DT is particularly useful for revealing threshold-dependent behavior [34], for
 223 instance, determining the optimal pH or adsorbent dosage beyond which removal efficiency plateaus. Its
 224 transparency makes it ideal for understanding mechanistic trends in adsorption systems. To determine estimated
 225 outputs, we usually average the true outputs of training samples within a terminal node [35]:

226
$$\hat{y}_j = \frac{\sum_{i \in t_j} Y_j}{|t_j|} \quad (1)$$

227 Where t_j =leaf node j, and $|t_j|$ = total number of datapoints/samples in the leaf node j. The split criteria of the
 228 decision tree are based on the impurity measure with the least squares deviation [36]

229
$$I(t_j) = \sum_{i \in t_j} (y_i - \hat{y}_j)^2 \quad (2)$$

230 Where $I(t_j)$ =the impurity measure at node j. Using the least square deviation, the splitting criteria are calculated
 231 as follows:

232
$$\Delta I = I(t_p) - P_l I(t_l) - P_r I(t_r) \quad (3)$$

233 Where t_l and t_r = two child nodes of t_p = parent node. The left child node assigned with proportions of data is
 234 represented by P_l , and the right child node assigned with proportions of data is represented by P_r .

235 2.3.2 Ensemble Learning Tree (ELT)

236 The Ensemble Learning Tree approach enhances predictive robustness by aggregating multiple weak learners to
 237 form a stronger composite model [37]. This ensemble strategy reduces overfitting, mitigates noise sensitivity, and
 238 improves overall model generalization, an essential feature when dealing with complex, nonlinear adsorption
 239 datasets [38]. In the current study, ELT was adopted to improve accuracy and stability in predicting adsorption
 240 performance across varying conditions. By averaging or combining outputs from several individual models, the
 241 ensemble method captures diverse feature interactions, making it effective for systems where adsorption behavior
 242 depends on multiple correlated factors such as ionic strength and molecular size.

243 2.3.3 Gaussian Process Regression (GPR)

244 Gaussian Process Regression was integrated into the hybrid model due to its probabilistic and non-parametric
 245 nature, allowing it to represent complex functional relationships between input variables and adsorption outcomes
 246 [39]. GPR not only provides accurate predictions but also quantifies uncertainty [40], which is particularly
 247 valuable for experimental adsorption data that may exhibit variability due to surface heterogeneity or adsorbate–
 248 adsorbent interactions. Its kernel-based approach enables modelling of nonlinear adsorption dynamics, making it
 249 a strong candidate for capturing the underlying physicochemical processes in biochar-based adsorption systems
 250 for dyes and proteins. The Gaussian process $t(u)$ is parameterized by two independent variables, the mean function
 251 $m(u)$ and the kernel function, also known as the covariance function $d(u, u')$, which are each evaluated for the
 252 instances u and u' , respectively (u) [41]. The equations below provide definitions for these two functions.

253
$$m(u) = E(t(u))$$

254
$$Cov(t(u), t(u')) = d(u, u'; \sigma) = E((t(u) - m(u))(t(u') - m(u')))$$

255 Where, σ = model hyperparameters that must be adjusted. Mathematically Gaussian process $t(u)$ is represented as

256
$$t(u) \sim GP(m(u), k(u, u'))$$

257 where GP denotes the Gaussian process model This implies that $t(u)$ is a probabilistic function where, $m(u)$
258 =Gaussian mean and $d(u, u')$ =covariance function.

259

260

261 2.3.3 Support Vector Machine (SVM)

262 Support Vector Machine was utilized for its superior performance in handling nonlinear regression tasks and its
263 ability to model high-dimensional feature spaces effectively [42]. Through kernel transformations, SVM can map
264 input parameters, such as solution chemistry, adsorbent properties, and operational conditions, into higher
265 dimensions where linear separation or regression becomes feasible. In the context of adsorption, SVM excels at
266 modelling complex sorption mechanisms and capturing multivariate dependencies between process parameters
267 and adsorption capacity [43]. Its robustness against overfitting and strong generalization ability makes it a key
268 component of the hybrid framework. Enhancing SVMs with kernels improves their flexibility and simplifies
269 handling nonlinear tasks. The equations defining the prediction function for the target output differ between a
270 linear support vector machine and a nonlinear SVM (including quadratic and cubic variations) [44].

$$271 \quad y(x) = \sum_{u=1}^U (a_u - a_u^*) (x'_u, x) + b \# (7)$$

$$272 \quad y(x) = \sum_{u=1}^U (a_u - a_u^*) P(x'_u, x) + b \# (8)$$

273 where, x_u =observed predictors, a_u and a_u^* =non-negative multiplier, b =random error term, P =Gram matrix of size
274 $u * u$ that consists of elements $p_{ij} = P(x_i, x_j)$.

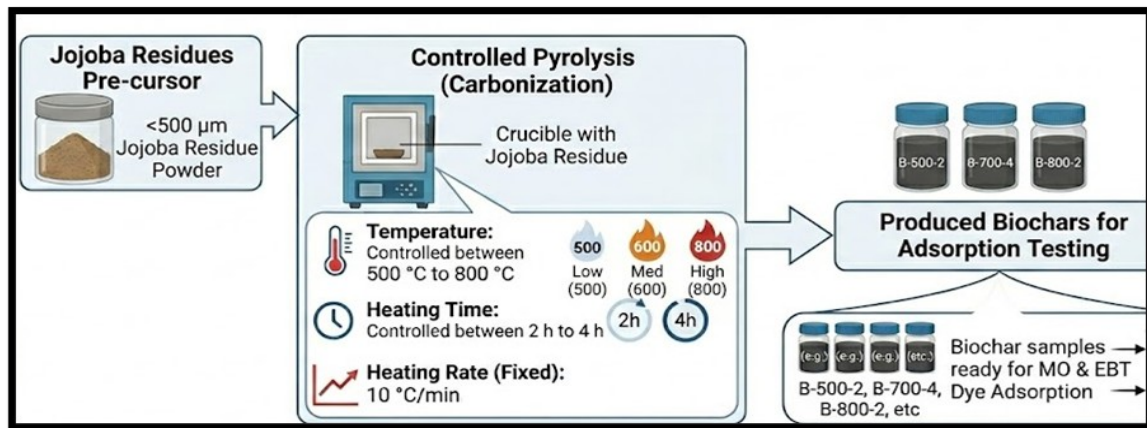
275 2.5. Optimization strategies

276 To further refine model performance and identify optimal parameter configurations, Bayesian optimization (BO)
277 was implemented as the optimization strategy. BO is a data-efficient, probabilistic approach that iteratively
278 explores the hyperparameter space to locate the best-performing model settings with minimal computational cost
279 [45]. Unlike exhaustive search methods such as grid or random search, BO constructs a surrogate model of the
280 objective function and continuously updates it using prior evaluations [46] . This enables a balanced trade-off
281 between exploration (testing new regions of the parameter space) and exploitation (refining known promising
282 areas). In this study, BO was employed to systematically optimize each ML model's hyperparameters, ensuring
283 convergence toward the global optimum for adsorption prediction accuracy. This strategy significantly improved
284 predictive performance while maintaining computational efficiency, making it well-suited for complex, nonlinear
285 adsorption datasets. The utilized hyper tuning parameters for selected ML models are provided in Table S2.

286 2.6. Production of biochar

287 In this study, biochar was produced from jojoba residues at different temperatures and heating times to
288 experimentally validate the developed ML models. The jojoba residues were obtained after pressing oil from
289 jojoba seeds, by crushing and sieving through a 500-micron mesh. The residues were pyrolyzed using a muffle

290 furnace at a temperature of (500-800) °C, heating time (2-4) h, and a fixed heating rate of 10 °C/min (Figure 4).
 291 The produced biochar was then tested for the adsorption of anionic dyes.



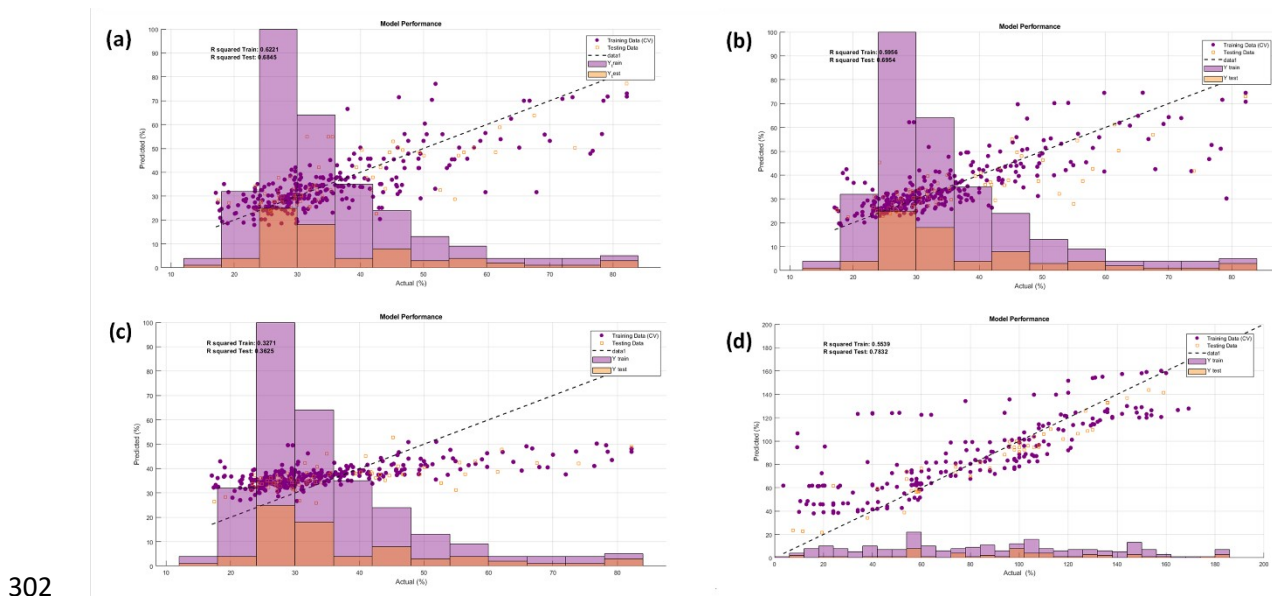
292

293

Figure 4. Production of biochar from jojoba residues.

294 **3. Results and discussion**

295 The selected models were trained and tested by using the obtained dataset, as shown in Figure 5. After applying
 296 the four ML models (DT, GPR, SVM, and ELT) and optimizing using BO, the results are provided in Table 1.
 297 The results show that the DT model is the least effective, underfitting the data and exhibiting very low explanatory
 298 power on both the training and test datasets. Followed by GPR, which had a slightly better result but only
 299 explained about 33% of the variance. SVM is not better than DT, explaining only 22% of the variance and showing
 300 weak predictive capability and overfitting. ELT has performed best among all ML models and improved R^2 on
 301 the test dataset. The dataset shows overfitting in some values, but overall, the model fits well.



302

303 **Figure 5.** Model training and testing dataset optimized utilizing four different ML models: (a) DT, (b) GPR, (c)
 304 SVM, and (d) ELT.

305

306

307

308

Table 1. Model training and testing dataset utilizing four different ML models.

| Models | | Before optimization | | After optimization | | Performance metrics | | | |
|--------|-------|---------------------|---------|--------------------|--------|---------------------|---------|--------|---------|
| | | R^2 | RMSE | R^2 | RMSE | MAE | EVS | MAPE | RSR |
| DT | Train | 0.1212 | 17.251 | 0.1816 | 11.608 | 7.9411 | 0.18161 | 22.867 | 0.90313 |
| | Test | 0.2175 | 18.214 | 0.1595 | 13.639 | 9.6844 | 0.1743 | 24.227 | 0.91055 |
| GPR | Train | 0.1254 | 15.257 | 0.3345 | 10.467 | 7.234 | 0.33479 | 20.822 | 0.81441 |
| | Test | 0.2954 | 17.8154 | 0.33377 | 12.143 | 8.4353 | 0.35124 | 21.125 | 0.81069 |
| SVM | Train | 0.1595 | 13.254 | 0.2236 | 11.306 | 8.5821 | 0.2364 | 26.324 | 0.87966 |
| | Test | 0.1621 | 17.215 | 0.22371 | 13.108 | 10.382 | 0.22526 | 27.624 | 0.8751 |
| ELT | Train | 0.4487 | 84.2147 | 0.56672 | 76.433 | 34.379 | 0.56672 | 48.528 | 0.65696 |
| | Test | 0.6421 | 45.251 | 0.78345 | 38.472 | 23.077 | 0.79312 | 21.882 | 0.4169 |

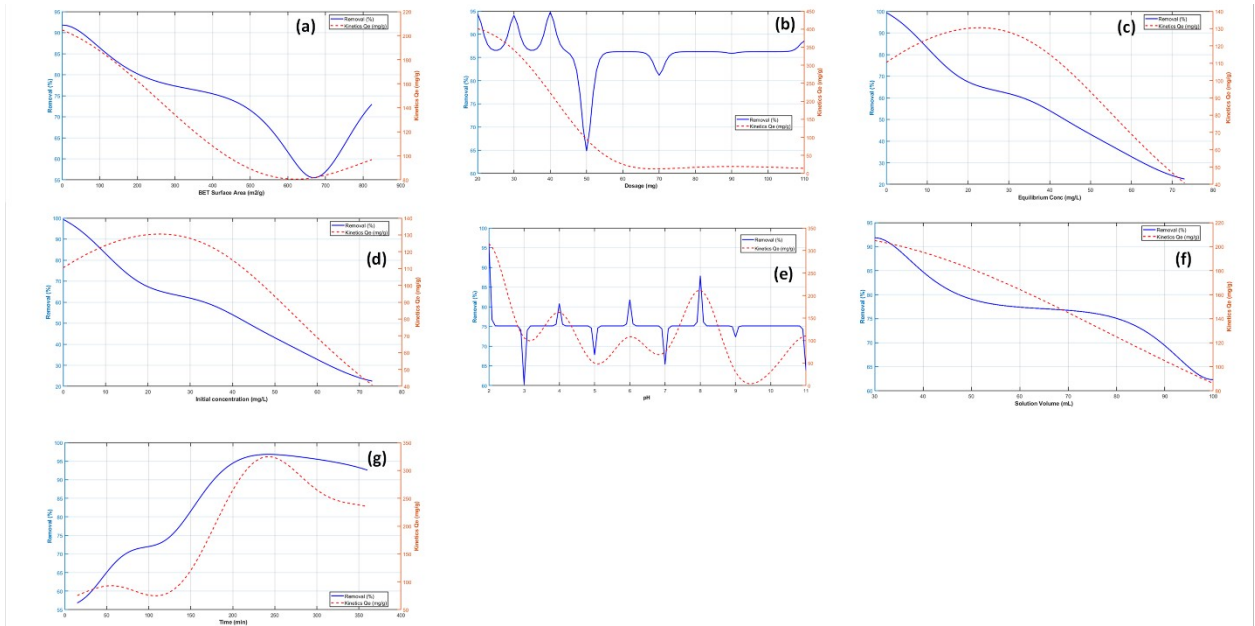
309

310 2D partial dependence plots

311 Machine Learning Models applied to the tabular dataset can be explained using Partial dependence plots (PDPs).
 312 They provide information on the impact of the input feature or features on the prediction of the output feature or
 313 features [47].

314 In this regard, 2D- PDPS of the input features (BET surface area, dosage of anionic dyes and proteins, equilibrium
 315 concentration, initial concentration, filtration material, pH of the solution, solution volume and time) are
 316 developed using the ELT model against the output features (Kinetics Q_e and adsorption Capacity) as shown in
 317 Figure 6. A decreasing trend is observed in both adsorption Capacity and Kinetics Q_e with the increase in the BET
 318 surface area to about 600 m^2/g after which it starts to increase. Adsorption capacity of the adsorbent and kinetics
 319 Q_e of materials are not solely dependent on the BET surface area, but also depend on the surface chemistry,
 320 molecule size of the anionic dyes and proteins and surface morphology of the adsorbent material. the U shape
 321 plot for this well describes the above phenomenon [48]. Adsorption capacity shows an oscillating trend with the
 322 increase of the dosage of the pollutants. Initially, at low pollutant dosage, there are abundant adsorption sites, but
 323 as the dosage increases, these sites become saturated with pollutants. The availability of the multilayer adsorbent
 324 enhances adsorption capacity at higher pollutant dosages, and similarly, Q_e Kinetics is affected in the same way
 325 [49]. PDP generated using the ELT ML model describes the same behaviour. A non-monotonic trend is observed
 326 in the PDP of the initial concentration against the kinetics Q_e . Raising the equilibrium concentration increases Q_e
 327 to about 20 mg/L, after which it declines due to the abundance of adsorbent sites [22]. An inverse relationship is
 328 observed between the adsorption capacity and the equilibrium concentration. A linear trend is observed in a PDP
 329 of initial concentration and Kinetics Q_e aligned with the established understanding of enhanced mass transfer
 330 driving force and abundance of the dye molecules. While adsorption capacity shows oscillatory behaviour, this
 331 arises from the interactions among the complex features captured by the model. This is the common trend that can
 332 be observed in water treatment studies where Kinetics Q_e is enhanced by increasing the initial concentration and
 333 maintaining the adsorption capacity till saturation [49]. The dependence of adsorption behaviour on solution pH
 334 is revealed by the PDP. At high acidic conditions (\sim pH 2-3), the model predicts higher Kinetics Q_e values,
 335 indicating enhanced electrostatic attraction between the anionic dye molecules and the positively charged
 336 adsorbent surface. Further increasing the pH generates negative surface charges that repel the anionic dye ions.

337 Oscillatory peaks in adsorption capacity around pH 4, 6, and 8 indicate optimal charge-solution conditions,
 338 followed by a decline under strong alkaline conditions [50]. The PDP observes a negative effect of increasing
 339 solution volume on adsorption capacity. Adsorption capacity starts just above 90% at 30 mL of the solution
 340 volume and decreases gradually to form a plateau around 60 to 75 mL of solution volume and drops sharply to
 341 65% capacity after 85 mL of Solution volume. Kinetics Qe behaves in a similar fashion, dropping from around
 342 200 mg/g to 90 mg/g by increasing the solution volume from 30 mL to 100 mL. This is due to dilution-enhanced
 343 reduction in the driving force of mass transfer, leading to fewer dye molecules available for the per unit mass of
 344 the adsorbent.



345
 346 **Figure 6.** 2D PDPs of adsorption removal vs experimental conditions: BET surface area (a), dosage (b),
 347 equilibrium concentration (c), initial concentration (d), pH (e), solution volume (f), and time (g).

348 3D partial dependence plots

349 Similarly, 3D PDP plots were also obtained as shown in Figure S3 (a-f). From the results, it can be inferred that
 350 adsorption % is more sensitive to pH, adsorbent dosage, and BET surface area due to synergistic interactions. 3D
 351 PDPs show that the increasing trend of removal efficiency is observed with higher dosage because of the
 352 availability of more active sites, but as soon particle starts to saturate, diminishing returns [51]. Effect of pH on
 353 adsorption % and dosage was also studied using 3D PDP which reveal pH crucial role in optimizing electrostatic
 354 condition for enhanced removal even at moderate dosages while with poor pH selection could also results in
 355 degraded removal at higher dosages as well partial dependence of adsorption % on BET surface area and pH was
 356 developed, high surface area improves adsorption % due to excess binding sites and it could be enhanced using
 357 optimal pH window. Surface charge can be changed by maximizing the pH, which may render ineffective high
 358 surface area [52].

359 Sensitivity

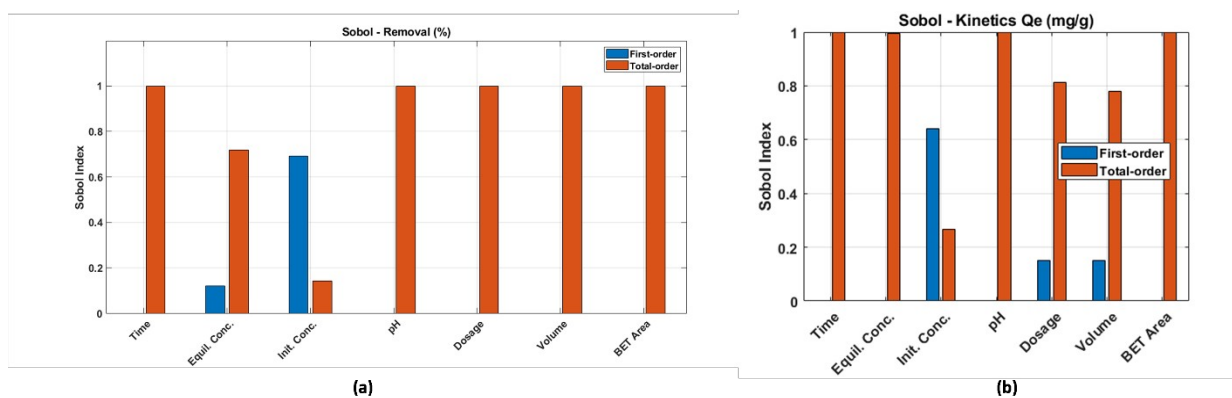
360 Sobol Global Sensitivity analyses were performed to assess the individual impact of each input feature on the
 361 adsorption capacity and kinetics Qe. Using this variance-based global sensitivity technique, the disintegration of
 362 the total variance of the output features can be evaluated as the individual and relative impacts of input features

363 on the total variance, on a scale of 0 to 1. Direct influence of the input feature is the first-order Sobol index,
364 whereas the total order refers to the interaction-based influence of the input features on the total variance of the
365 Output [53].

366 Sensitivity patterns of all the input features with individual and relative Sobol index are shown in Figure 7 (a -b)
367 for adsorption capacity and Kinetics Q_e . Initial Concentration is the dominant first-order feature for both
368 adsorption capacity (Q_e) and kinetics, suggesting that the availability of active sites, driven by the concentration
369 gradient, controls adsorption efficiency independently. While the other input features show low first order
370 compared to initial concentration, their total order reaches unity, indicating that their interaction with the other
371 features strengthens their influence [54].

372 Model outputs are further tested for reliability and variability using kernel density estimates (KDEs) of adsorption
373 capacity and kinetics. These KDEs are developed based on separation methods (batch and sonication) and the
374 type of pollutant removed. While the pollutant distinctly affects the distribution of adsorption capacity and kinetics
375 (Q_e), the model depends on the type of pollutant being removed (Figure S4a). Adsorption capacity and Kinetics
376 distribution became narrower and higher for the sonication method, predicting model performance being more
377 concise compared to the batch method (Figure S4a) [55].

378 Monte Carlo simulations ($N=1000$), as shown in Figure S4b, are used to further quantify the prediction uncertainty
379 by selecting input parameters randomly not exceeding their experimental limits and propagating through the
380 optimised ML model. A narrow distribution (mean $\approx 90\%$, 95 % CI $\approx 85-95\%$) of the predicted adsorption
381 capacity validates the model's accuracy and reliability. On the other hand, kinetics Q_e predictions are broader and
382 right-skewed (mean ≈ 500 mg/g, 95 % CI $\approx 100-2000$ mg/g), reflecting the high dependence and sensitivity on
383 the input fluctuations. These results suggest that more Kinetics Q_e data is required to eliminate the uncertainty,
384 along with affirmation of the prediction robustness of the ML model for adsorption capacity [56].



385 (a) 386 **Figure 7.** Sobol sensitivity patterns of input features for adsorption removal capacity and kinetics Q_e .

387 **Experimental Validation**

388 Table 2 shows the experimental and predicted results for the % removal and kinetic adsorption capacity from MO
389 and EBT dyes removal using different joboba-derived biochar produced using different temperatures (500-800 °C)
390 and heating times (2-4 h). As shown, increasing the pyrolysis temperature from 500°C to 800°C results in a
391 significant increase in % removal for both methyl orange (MO) and Eriochrome black T (EBT) dyes. In addition,
392 a slight increase in adsorption performance was observed when the pyrolysis heating time increased from 2h to

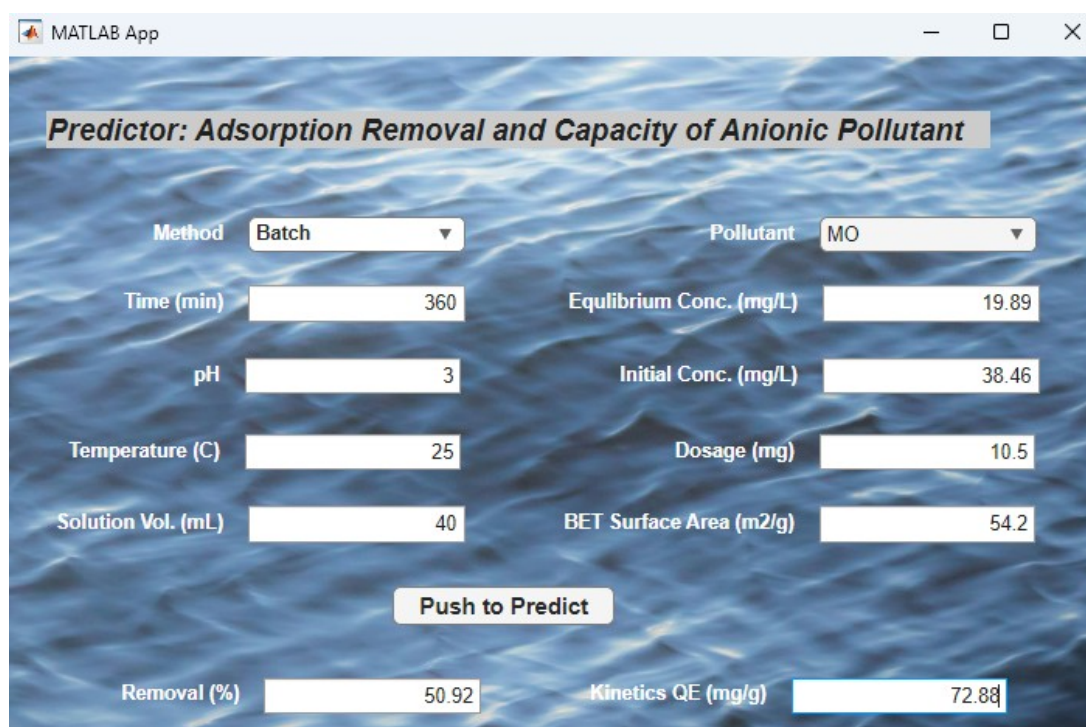
4h. The increase in adsorption of dyes at higher biochar pyrolysis temperatures is mainly associated with the development of a porous surface structure and an increase in specific surface area, resulting from the complete degradation of jojoba residues [57]. The porous surface serves as active binding sites for dye molecules via pore-filling behavior [58]. Furthermore, the high-temperature biochar (700-800°C) exhibited high aromaticity, which dominated pi-pi interactions between the biochar's carbon layers and the aromatic rings of the dyes. Specifically, EBT dye exhibits a higher adsorption capacity (Q_e) than MO due to its smaller molecular size, which allows it to penetrate biochar pores more easily via a pore-filling mechanism. Previous studies also indicated that the formation of porous and graphite structures at 700-800°C promoted pore filling and hydrophobic interactions as dominant adsorption mechanisms [59]. The comparison between experimental data and ML predictions reveals a strong correlation, suggesting that the ML model successfully captures the non-linear relationship between production parameters and adsorption efficiency. The ML model's ability to mirror the "plateau" or "steep increase" in experimental % removal indicates that it accurately weights pyrolysis temperature as the most critical feature relative to heating time. Overall, the integration of ML validates the experimental results, confirming that the pyrolysis parameters are reliable predictors for the design of high-performance biochars for effective treatment of dye-contaminated wastewater.

Table 2. Comparison of ML-predicted results with experimental values at different conditions for removing anionic dyes after 6 h using different jojoba-derived biochars (fixed conditions: pH = 3, temperature = 25 °C, solution volume = 40 mL).

| Pollutant | Material | Initial concentration (mg/L) | Dosage (mg) | Experimental | | Predicted | | % Error | |
|-----------|----------|------------------------------|-------------|--------------|-----------------------|-------------|-----------------------|-------------|-----------------------|
| | | | | Removal % | Kinetics Q_e (mg/g) | Removal (%) | Kinetics Q_e (mg/g) | Removal (%) | Kinetics Q_e (mg/g) |
| EBT | B-700-4 | 48.88 | 10.75 | 25.51 | 46.40 | 24.31 | 45.20 | 4.71 | 2.59 |
| MO | B-700-4 | 38.46 | 10.71 | 21.48 | 30.85 | 23.51 | 32.18 | 9.47 | 4.31 |
| MO | B-500-2 | 38.46 | 10.5 | 48.28 | 70.74 | 50.92 | 72.88 | 5.46 | 3.02 |
| EBT | B-500-2 | 48.88 | 10.77 | 9.80 | 17.79 | 10.50 | 18.81 | 7.15 | 5.73 |
| EBT | B-500-4 | 48.88 | 10.7 | 15.22 | 27.81 | 14.91 | 29.15 | 2.04 | 4.81 |
| EBT | B-600-2 | 48.88 | 10.46 | 10.11 | 18.89 | 9.50 | 17.16 | 6.00 | 9.16 |
| EBT | B-700-2 | 48.88 | 10.17 | 16.76 | 32.21 | 16.42 | 32.73 | 2.00 | 1.61 |
| EBT | B-800-2 | 48.88 | 10.42 | 24.71 | 46.37 | 24.06 | 47.53 | 2.64 | 2.50 |
| EBT | B-800-4 | 48.88 | 10.41 | 29.66 | 55.72 | 31.35 | 58.48 | 5.68 | 4.96 |
| MO | B-500-4 | 38.46 | 10.69 | 24.05 | 34.61 | 26.37 | 31.91 | 9.64 | 7.81 |
| MO | B-600-2 | 38.46 | 10.52 | 52.29 | 76.46 | 50.51 | 78.66 | 3.40 | 2.87 |
| MO | B-600-4 | 38.46 | 10.09 | 22.05 | 33.62 | 23.31 | 35.15 | 5.72 | 4.56 |
| MO | B-700-2 | 38.46 | 10.63 | 32.24 | 46.66 | 33.64 | 45.51 | 4.34 | 2.47 |
| MO | B-800-2 | 38.46 | 10.18 | 38.85 | 58.70 | 40.12 | 57.32 | 3.28 | 2.36 |
| MO | B-800-4 | 38.46 | 10.29 | 19.68 | 29.43 | 21.44 | 27.81 | 8.93 | 5.49 |

To facilitate the practical implementation of the developed machine learning framework, a graphical user interface (GUI) was designed using MATLAB R2021b, as shown in Figure 8. The GUI integrates the optimized Ensemble Learning Tree (ELT) model, allowing users to rapidly predict adsorption removal efficiency and adsorption capacity under user-defined experimental conditions. The developed interface provides an accessible platform that eliminates the need for direct interaction with the underlying machine learning code, enabling researchers and engineers to perform rapid assessments of adsorption performance. The GUI was developed using MATLAB's App Designer, which supports interactive user input and real-time prediction using the trained ML model. The interface consists of several input panels corresponding to the key operational parameters used during model training. These parameters include the solution pH, adsorbent dosage, BET surface area of the adsorbent, initial pollutant concentration, equilibrium concentration, solution volume, contact time, and adsorbent material type.

422 Each parameter can be entered manually within the range of values used during model training to ensure reliable
423 predictions. Once the experimental parameters are specified, the GUI processes the input data and passes it to the
424 trained ELT regression model, which computes the predicted adsorption performance. The interface subsequently
425 displays two main outputs, i.e., adsorptive removal (%) and capacity (q_e , mg/g). These predictions are generated
426 instantaneously, enabling users to evaluate how variations in operational parameters influence adsorption
427 performance without conducting time-consuming laboratory experiments. The developed GUI demonstrates the
428 potential of integrating machine learning models with user-friendly software tools to bridge the gap between data-
429 driven modelling and practical environmental engineering applications.



430

431 **Figure 8.** Screenshot of the GUI program developed for predictive removal of anionic pollutants via selected
432 carbonaceous adsorbents.

433 Conclusion

434 This study presents a machine learning-assisted strategy for predicting adsorption performance and optimizing
435 operational conditions for the removal of anionic pollutants from aqueous systems. A comprehensive experimental
436 dataset comprising multiple pollutants, adsorbent materials, and operational parameters was used to develop
437 predictive models utilizing Decision Tree, Gaussian Process Regression, Support Vector Machine, and Ensemble
438 Learning Tree algorithms. Bayesian optimization significantly improved model performance, with the optimized
439 Ensemble Learning Tree demonstrating the highest predictive accuracy and the strongest capability to capture
440 nonlinear adsorption behavior. Model interpretation through partial dependence analysis and Sobol sensitivity
441 assessment revealed that adsorption performance is primarily governed by initial pollutant concentration, pH,
442 adsorbent dosage, and BET surface area. These analyses provide valuable insights into the complex interactions
443 between operational conditions and adsorption efficiency. The reliability of the developed ML framework was
444 further validated experimentally using jobo-derived biochar for the removal of methyl orange and Eriochrome
445 Black T dyes, where predicted results showed strong agreement with experimental observations. The integration

446 of experimental data, advanced machine learning modelling, and uncertainty analysis demonstrates a robust
447 predictive framework for adsorption-based water treatment systems. Furthermore, the development of a graphical
448 user interface enables rapid estimation of adsorption performance under different conditions, offering a practical
449 decision-support tool for process design. This work highlights the potential of data-driven approaches to accelerate
450 the development and optimization of efficient adsorbent materials for wastewater remediation.

451 **Acknowledgements**

452 The authors are thankful to the National University of Sciences and Technology (NUST) Research Directorate,
453 HEC, and NRPDU through Project No. 6020 for all the technical assistance and financial support. The authors also
454 gratefully acknowledge the support from the European Just Transition Fund within the Operational Programme:
455 Just Transition under the aegis of the Ministry of the Environment of the Czech Republic, project CirkArena
456 number CZ.10.03.01/00/22_003/0000045 and the Ministry of Education Youth and Sports of the Czech Republic,
457 Operational Programme Johannes Amos Comenius OP JAC "Application potential development in the field of
458 polymer materials in the context of circular economy compliance (POCEK)", number
459 CZ.02.01.01/00/23_021/0009004. The authors are further grateful for co-funding from the development process
460 of the Centre of Polymer Systems, Tomas Bata University in Zlin, program DKRVO (RP/CPS/2024-28/002) and
461 (RP/CPS/2024-28/007), supported by the Ministry of Education, Youth and Sports of the Czech Republic.

462 **CrediT authorship contribution statement**

463 **Hamza Ul Haq:** Conceptualization, Methodology, Investigation, Formal analysis, Data curation, Writing-
464 original draft, Writing- Review & editing. **Muhammad Yasir:** Methodology, Visualization, Formal analysis,
465 Data curation, Writing- Review & editing. **Muhammad Nouman Aslam Khan:** Software, Formal analysis, Data
466 curation, Supervision, Writing- Review & editing. **Jawad Gul:** Data curation, Writing- Review & editing.
467 **Mukarram Zubair:** Investigation, validation, formal analysis. **Vladimír Sedlařík:** Supervision, Project
468 administration, Funding acquisition, Writing- Review & editing. **Hassan Ali:** Writing- Review & editing,
469 Investigation. **Nasir M. Ahmad:** Supervision, Resources, Project administration, Funding acquisition, Writing-
470 Review & editing.

471 **References**

- 472 [1] P. Babuji, S. Thirumalaisamy, K. Duraisamy, G. Periyasamy, Human Health Risks due to Exposure to
473 Water Pollution: A Review, *Water* 15 (2023) 2532. <https://doi.org/10.3390/w15142532>.
- 474 [2] A. Gezahegn, L.B. Merga, S. Mammo, Industrial effluents caused environmental pollution and its
475 potential ecological and human health impacts in Ethiopia: A review, *Waste Management Bulletin* 3
476 (2025) 100240. <https://doi.org/10.1016/j.wmb.2025.100240>.
- 477 [3] K. Sathya, K. Nagarajan, G. Carlin Geor Malar, S. Rajalakshmi, P. Raja Lakshmi, A comprehensive
478 review on comparison among effluent treatment methods and modern methods of treatment of industrial
479 wastewater effluent from different sources, *Appl Water Sci* 12 (2022) 70. <https://doi.org/10.1007/s13201-022-01594-7>.
- 481 [4] G.M. Filippelli, M.P. Taylor, Addressing Pollution-Related Global Environmental Health Burdens,
482 *GeoHealth* 2 (2018) 2–5. <https://doi.org/10.1002/2017GH000119>.
- 483 [5] G. Yumnam, Y. Gyanendra, C.I. Singh, A systematic bibliometric review of the global research dynamics
484 of United Nations Sustainable Development Goals 2030, *Sustainable Futures* 7 (2024) 100192.
485 <https://doi.org/10.1016/j.sfr.2024.100192>.
- 486 [6] S. Duan, H. Dong, C. Jiang, H. Liang, L. Jiang, Q. Xu, X. Cheng, Z. Qiang, Removal of particulate matter
487 and dissolved organic matter from sedimentation sludge water during pre-sedimentation process:
488 Performances and mechanisms, *Journal of Environmental Sciences* 148 (2025) 409–419.
489 <https://doi.org/10.1016/j.jes.2023.11.026>.

- 490 [7] S. Jamil, P. Loganathan, J. Kandasamy, A. Listowski, J.A. McDonald, S.J. Khan, S. Vigneswaran,
491 Removal of organic matter from wastewater reverse osmosis concentrate using granular activated carbon
492 and anion exchange resin adsorbent columns in sequence, *Chemosphere* 261 (2020) 127549.
493 <https://doi.org/10.1016/j.chemosphere.2020.127549>.
- 494 [8] E. Topkaya, A. Arslan, S. Veli, S. Kuru, M. Sezer, Removal of Microplastics By Ozone Oxidation from
495 Urban Wastewater Using Taguchi Experimental Design, *Water Air Soil Pollut* 236 (2025) 606.
496 <https://doi.org/10.1007/s11270-025-08249-8>.
- 497 [9] J.-H. Joo, S.-H. Kim, J.H. Kim, H.-J. Kang, J.H. Lee, H.-J. Jeon, Y.H. Jang, J.-H. Lee, S.-Y. Lee, S.-J.
498 Park, M.-K. Seo, Recent advances in activated carbon fibers for pollutant removal, *Carbon Lett.* 35 (2025)
499 21–44. <https://doi.org/10.1007/s42823-024-00803-4>.
- 500 [10] S.M. Chistie, S.U. Naik, P. Rajendra, Apeksha, R.K. Mishra, G. Albasher, S. Chinnam, G.P. Jeppu, Z.
501 Arif, J. Hameed, Production and characterization of magnetic Biochar derived from pyrolysis of waste
502 areca nut husk for removal of methylene blue dye from wastewater, *Sci Rep* 15 (2025) 23209.
503 <https://doi.org/10.1038/s41598-025-03359-z>.
- 504 [11] R. Shahi, M. Khatamian, Synthesis of magnetic borosilicate zeolite/graphene quantum dots
505 nanocomposites for removal of nitrate and organic pollutants from water, *Sci Rep* 15 (2025) 20726.
506 <https://doi.org/10.1038/s41598-025-07746-4>.
- 507 [12] L.N. Munuhe, E.S. Madivoli, D.M. Nzilu, P.N. Lemeitaron, P.K. Kimani, Advances in Adsorbent
508 Materials for Pharmaceutical Pollutant Removal: A Review of Occurrence, Fate, and State-of-the-Art
509 Remediation, *Journal of Chemistry* 2025 (2025) 4477822. <https://doi.org/10.1155/joch/4477822>.
- 510 [13] R.B. Phillips, R.R. James, M.L. Magnuson, Functional categories of microbial toxicity resulting from
511 three advanced oxidation process treatments during management and disposal of contaminated water,
512 *Chemosphere* 238 (2020) 124550. <https://doi.org/10.1016/j.chemosphere.2019.124550>.
- 513 [14] W. Ashraf, D. Sharma, A. Khan, M. Khanuja, Green Carbon Dots as Adsorbents for Removal of Toxic
514 Chemicals, in: S.U. Islam, C.M. Hussain (Eds.), ACS Symposium Series, American Chemical Society,
515 Washington, DC, 2025: pp. 141–160. <https://doi.org/10.1021/bk-2025-1506.ch006>.
- 516 [15] P. Waribam, T.R. Katugampalage, M. Ogawa, P. Opaprakasit, W. Chooaksorn, P. Sooksanen, P. Puathawee,
517 P. Sreearunothai, Magnetic Metal–Organic Frameworks (MOFs) from Waste: A Solvent-Free Rapid
518 Synthesis of Green Catalyst for Environmental Cleanup, *ACS Sustainable Chem. Eng.* 13 (2025) 9576–
519 9587. <https://doi.org/10.1021/acssuschemeng.5c02222>.
- 520 [16] R. Natarajan, K. Saikia, S.K. Ponnusamy, A.K. Rathankumar, D.S. Rajendran, S. Venkataraman, D.B.
521 Tannani, V. Arvind, T. Somanna, K. Banerjee, N. Mohideen, V.K. Vaidyanathan, Understanding the
522 factors affecting adsorption of pharmaceuticals on different adsorbents – A critical literature update,
523 *Chemosphere* 287 (2022) 131958. <https://doi.org/10.1016/j.chemosphere.2021.131958>.
- 524 [17] R. Li, X. Cao, X. Fan, J. Shi, B. Meng, J. Zhang, Y. Wang, J. Du, X. Deng, C. Zheng, Study of the Factors
525 Influencing the Adsorption of Heavy Metal Pollutants in Water by Activated Carbon Gel Particles, *J.*
526 *Environ. Eng.* 150 (2024) 04024024. <https://doi.org/10.1061/JOEEDU.EEENG-7606>.
- 527 [18] P.B. Joshi, Navigating with chemometrics and machine learning in chemistry, *Artif Intell Rev* 56 (2023)
528 9089–9114. <https://doi.org/10.1007/s10462-023-10391-w>.
- 529 [19] A.K. Cheetham, R. Seshadri, Artificial Intelligence Driving Materials Discovery? Perspective on the
530 Article: Scaling Deep Learning for Materials Discovery, *Chem. Mater.* 36 (2024) 3490–3495.
531 <https://doi.org/10.1021/acs.chemmater.4c00643>.
- 532 [20] N. Li, S. Girhe, M. Zhang, B. Chen, Y. Zhang, S. Liu, H. Pitsch, A machine learning method to predict
533 rate constants for various reactions in combustion kinetic models, *Combustion and Flame* 263 (2024)
534 113375. <https://doi.org/10.1016/j.combustflame.2024.113375>.
- 535 [21] I. Malashin, V. Tynchenko, A. Gantimurov, V. Nelyub, A. Borodulin, Optimizing Neural Networks for
536 Chemical Reaction Prediction: Insights from Methylene Blue Reduction Reactions, *IJMS* 25 (2024) 3860.
537 <https://doi.org/10.3390/ijms25073860>.
- 538 [22] H. Ali, M. Yasir, H.U. Haq, A.C. Guler, M. Masar, M.N.A. Khan, M. Machovsky, V. Sedlarik, I. Kuritka,
539 Machine learning approach for photocatalysis: An experimentally validated case study of photocatalytic
540 dye degradation, *Journal of Environmental Management* 386 (2025) 125683.
541 <https://doi.org/10.1016/j.jenvman.2025.125683>.
- 542 [23] H. Ullah, S. Khan, X. Zhu, B. Chen, Z. Rao, N. Wu, A.M. Idris, Machine learning-aided biochar design
543 for the adsorptive removal of emerging inorganic pollutants in water, *Separation and Purification*
544 *Technology* 362 (2025) 131421. <https://doi.org/10.1016/j.seppur.2025.131421>.
- 545 [24] M.S. Johnson, W.H. Green, A machine learning based approach to reaction rate estimation, *React. Chem.*
546 *Eng.* 9 (2024) 1364–1380. <https://doi.org/10.1039/D3RE00684K>.
- 547 [25] M. Lambev, D. Dimitrova, S. Mihaylova, Machine Learning-Based Prediction of Rule Violations for
548 Drug-Likeness Assessment in Peptide Molecules Using Random Forest Models, *IJMS* 26 (2025) 8407.
549 <https://doi.org/10.3390/ijms26178407>.

- 550 [26] A. Tabet, T. Gebhart, G. Wu, C. Readman, M. Pierson Smela, V.K. Rana, C. Baker, H. Bulstrode, P.
551 Anikeeva, D.H. Rowitch, O.A. Scherman, Applying support-vector machine learning algorithms toward
552 predicting host–guest interactions with cucurbit[7]uril, *Phys. Chem. Chem. Phys.* 22 (2020) 14976–
553 14982. <https://doi.org/10.1039/C9CP05800A>.
- 554 [27] M. Abbod, N. Safaie, K. Gholivand, Genetic algorithm multiple linear regression and machine learning-
555 driven QSTR modeling for the acute toxicity of sterol biosynthesis inhibitor fungicides, *Heliyon* 10
556 (2024) e36373. <https://doi.org/10.1016/j.heliyon.2024.e36373>.
- 557 [28] M. Vera, J. Aguilar, S. Coronel, D. Juela, E. Vanegas, C. Cruzat, Machine learning for the adsorptive
558 removal of ciprofloxacin using sugarcane bagasse as a low-cost biosorbent: comparison of analytic,
559 mechanistic, and neural network modeling, *Environ Sci Pollut Res* 31 (2024) 48674–48686.
560 <https://doi.org/10.1007/s11356-024-34345-z>.
- 561 [29] A.A. Akinpelu, M.K. Nazal, M. Shafiullah, M.K. Islam, M.M. Islam, A. Rahman, S.M. Rahman, M.M.
562 Rahman, A Multivariate Machine Learning Model of Adsorptive Lindane Removal from Contaminated
563 Water, *Applied Sciences* 13 (2023) 7086. <https://doi.org/10.3390/app13127086>.
- 564 [30] J. Li, J. Wang, H. Mu, H. Hu, J. Wang, H. Ren, B. Wu, Prediction of Adsorptive Activities of MOFs for
565 Pollutants in Aqueous Phase Based on Machine Learning, *ACS EST Eng.* 3 (2023) 1258–1266.
566 <https://doi.org/10.1021/acsestengg.3c00086>.
- 567 [31] H. Ullah, S. Khan, B. Chen, A. Shahab, L. Riaz, L. Lun, N. Wu, Machine learning approach to predict
568 adsorption capacity of Fe-modified biochar for selenium, *Carbon Res.* 2 (2023) 29.
569 <https://doi.org/10.1007/s44246-023-00061-5>.
- 570 [32] E. Abbasi, M.R. Alavi Moghaddam, E. Kowsari, A systematic and critical review on development of
571 machine learning based-ensemble models for prediction of adsorption process efficiency, *Journal of*
572 *Cleaner Production* 379 (2022) 134588. <https://doi.org/10.1016/j.jclepro.2022.134588>.
- 573 [33] A. Gupta, K. Ghanshala, R.C. Joshi, Machine Learning Classifier Approach with Gaussian Process,
574 Ensemble boosted Trees, SVM, and Linear Regression for 5G Signal Coverage Mapping., *IJIMAI* 6
575 (2021) 156–163. <https://doi.org/10.9781/ijimai.2021.03.004>.
- 576 [34] E. Syguła, K. Piasecka, J. Łyczko, A. Białowiec, The potential of decision tree application in threshold
577 analysis of hazardous volatile organic compound release from biochar: Implications for environmental
578 risk assessment, *Science of The Total Environment* 998 (2025) 180252.
579 <https://doi.org/10.1016/j.scitotenv.2025.180252>.
- 580 [35] K. Kim, J. Hong, A hybrid decision tree algorithm for mixed numeric and categorical data in regression
581 analysis, *Pattern Recognition Letters* 98 (2017) 39–45. <https://doi.org/10.1016/j.patrec.2017.08.011>.
- 582 [36] J. Li, W. Zhang, T. Liu, L. Yang, H. Li, H. Peng, S. Jiang, X. Wang, L. Leng, Machine learning aided bio-
583 oil production with high energy recovery and low nitrogen content from hydrothermal liquefaction of
584 biomass with experiment verification, *Chemical Engineering Journal* 425 (2021) 130649.
585 <https://doi.org/10.1016/j.cej.2021.130649>.
- 586 [37] I. Bibers, O. Arreche, W. Alayed, M. Abdallah, Ensemble-IDS: An Ensemble Learning Framework for
587 Enhancing AI-Based Network Intrusion Detection Tasks, *Applied Sciences* 15 (2025) 10579.
588 <https://doi.org/10.3390/app151910579>.
- 589 [38] D.K. Jha, Smart screening of hydrogen storage capacities in MOFs using a tailored machine learning,
590 *Next Energy* 9 (2025) 100431. <https://doi.org/10.1016/j.nxener.2025.100431>.
- 591 [39] V.L. Deringer, A.P. Bartók, N. Bernstein, D.M. Wilkins, M. Ceriotti, G. Csányi, Gaussian Process
592 Regression for Materials and Molecules, *Chem. Rev.* 121 (2021) 10073–10141.
593 <https://doi.org/10.1021/acs.chemrev.1c00022>.
- 594 [40] Z.M. Yaseen, M.M. Hameed, Z.H. Doost, Validation of machine learning models for heavy metals
595 bioavailability prediction: A comparative study, *Journal of Environmental Chemical Engineering* 13
596 (2025) 116749. <https://doi.org/10.1016/j.jece.2025.116749>.
- 597 [41] E. Momeni, M.B. Dowlatshahi, F. Omidinasab, H. Maizir, D.J. Armaghani, Gaussian Process Regression
598 Technique to Estimate the Pile Bearing Capacity, *Arab J Sci Eng* 45 (2020) 8255–8267.
599 <https://doi.org/10.1007/s13369-020-04683-4>.
- 600 [42] X. Li, W. Sun, C. Qin, Y. Yan, L. Zhang, J. Tu, Evaluation of supervised machine learning regression
601 models for CFD-based surrogate modelling in indoor airflow field reconstruction, *Building and*
602 *Environment* 267 (2025) 112173. <https://doi.org/10.1016/j.buildenv.2024.112173>.
- 603 [43] S. Emamgholizadeh, B. Mohammadi, New hybrid nature-based algorithm to integration support vector
604 machine for prediction of soil cation exchange capacity, *Soft Comput* 25 (2021) 13451–13464.
605 <https://doi.org/10.1007/s00500-021-06095-4>.
- 606 [44] A. Bahadar, R. Kanthasamy, H.H. Sait, M. Zwawi, M. Algarni, B.V. Ayodele, C.K. Cheng, L.J. Wei,
607 Elucidating the effect of process parameters on the production of hydrogen-rich syngas by biomass and
608 coal Co-gasification techniques: A multi-criteria modeling approach, *Chemosphere* 287 (2022) 132052.
609 <https://doi.org/10.1016/j.chemosphere.2021.132052>.

- 610 [45] R. Guay-Hottin, L. Kardassevitch, H. Pham, G. Lajoie, M. Bonizzato, Robust prior-biased acquisition
611 function for human-in-the-loop Bayesian optimization, *Knowledge-Based Systems* 311 (2025) 113039.
612 <https://doi.org/10.1016/j.knosys.2025.113039>.
- 613 [46] B. Lei, T.Q. Kirk, A. Bhattacharya, D. Pati, X. Qian, R. Arroyave, B.K. Mallick, Bayesian optimization
614 with adaptive surrogate models for automated experimental design, *Npj Comput Mater* 7 (2021) 194.
615 <https://doi.org/10.1038/s41524-021-00662-x>.
- 616 [47] D. Kerrigan, B. Barr, E. Bertini, PDPilot: Exploring Partial Dependence Plots Through Ranking, Filtering,
617 and Clustering, *IEEE Trans. Visual. Comput. Graphics* 31 (2025) 7377–7390.
618 <https://doi.org/10.1109/TVCG.2025.3545025>.
- 619 [48] I. Karume, S. Bbumba, S. Tewolde, I.Z.T. Mukasa, M. Ntale, Impact of carbonization conditions and
620 adsorbate nature on the performance of activated carbon in water treatment, *BMC Chemistry* 17 (2023)
621 162. <https://doi.org/10.1186/s13065-023-01091-1>.
- 622 [49] N. Hamri, A. Imessaoudene, A. Hadadi, S. Cheikh, A. Boukerroui, J.-C. Bollinger, A. Amrane, H.
623 Tahraoui, H.N. Tran, A.O. Ezzat, H.A. Al-Lohedan, L. Mouni, Enhanced Adsorption Capacity of
624 Methylene Blue Dye onto Kaolin through Acid Treatment: Batch Adsorption and Machine Learning
625 Studies, *Water* 16 (2024) 243. <https://doi.org/10.3390/w16020243>.
- 626 [50] W. Zhu, F. Chen, L. Ye, X. Yang, Y. Song, H. Wang, Methylene blue and acid red adsorption on biochar
627 made from modified sugarcane bagasse: A dynamic, equilibrium, and thermodynamic investigation,
628 *Adsorption Science & Technology* 42 (2024) 02636174241273522.
629 <https://doi.org/10.1177/02636174241273522>.
- 630 [51] Y. Luo, Z. Zheng, P. Wu, Y. Wu, Effect of different direct revegetation strategies on the mobility of heavy
631 metals in artificial zinc smelting waste slag: Implications for phytoremediation, *Chemosphere* 286 (2022)
632 131678. <https://doi.org/10.1016/j.chemosphere.2021.131678>.
- 633 [52] M. Bellaj, K. Aziz, M. El Achaby, M. El Haddad, L. Gebrati, T.A. Kurniawan, Z. Chen, P.-S. Yap, F. Aziz,
634 Cationic and anionic dyes adsorption from wastewater by clay-chitosan composite: An integrated
635 experimental and modeling study, *Chemical Engineering Science* 285 (2024) 119615.
636 <https://doi.org/10.1016/j.ces.2023.119615>.
- 637 [53] W. Zouhri, L. Homri, J.-Y. Dantan, Handling the impact of feature uncertainties on SVM: A robust
638 approach based on Sobol sensitivity analysis, *Expert Systems with Applications* 189 (2022) 115691.
639 <https://doi.org/10.1016/j.eswa.2021.115691>.
- 640 [54] H. Zheng, X. Meng, Y. Yang, J. Chen, S. Huo, Bifunctional photocatalytic nanofiltration membranes with
641 immobilized BaTiO₃/Ti₃C₂T catalysts for the simultaneous separation and degradation of azo
642 compounds, *Journal of Environmental Chemical Engineering* 11 (2023) 110064.
643 <https://doi.org/10.1016/j.jece.2023.110064>.
- 644 [55] J. Latif, N. Chen, A. Saleem, K. Li, J. Qin, H. Yang, H. Jia, Machine learning for persistent free radicals in
645 biochar: dual prediction of contents and types using regression and classification models, *Carbon Res.* 3
646 (2024) 39. <https://doi.org/10.1007/s44246-024-00125-0>.
- 647 [56] S. Chheda, W. Jeong, N. Hanikel, L. Gagliardi, J.I. Siepmann, Monte Carlo Simulations of Water
648 Adsorption in Aluminum Oxide Rod-Based Metal–Organic Frameworks, *J. Phys. Chem. C* 127 (2023)
649 7837–7851. <https://doi.org/10.1021/acs.jpcc.3c00354>.
- 650 [57] M. Zubair, N.D. Mu'azu, N. Jarrah, N.I. Blaisi, H.A. Aziz, M. A. Al-Harhi, Adsorption Behavior and
651 Mechanism of Methylene Blue, Crystal Violet, Eriochrome Black T, and Methyl Orange Dyes onto
652 Biochar-Derived Date Palm Fronds Waste Produced at Different Pyrolysis Conditions, *Water Air Soil
653 Pollut* 231 (2020) 240. <https://doi.org/10.1007/s11270-020-04595-x>.
- 654 [58] M. Zeeshan, T. Javed, C. Kumari, A. Thumma, M. Wasim, M.B. Taj, I. Sharma, M.N. Haider, M. Batool,
655 Investigating the interactions between dyes and porous/composite materials: A comprehensive study,
656 *Sustainable Chemistry for the Environment* 9 (2025) 100217.
657 <https://doi.org/10.1016/j.scenv.2025.100217>.
- 658 [59] S. Qiu, Q. Li, X. Li, J. Ma, L. Wu, X. Xie, L. Wu, S. Askari, N. Dewangan, J. Ashok, X. Gao, S. Kawi,
659 Biomass-Derived Carbon Materials for the Adsorption of Organic Pollutants, *Advanced Sustainable
660 Systems* 8 (2024) 2300340. <https://doi.org/10.1002/adsu.202300340>.
- 661